International Journal of Solids and Structures 47 (2010) 1641–1650

Contents lists available at ScienceDirect

International Journal of Solids and Structures

journal homepage: www.elsevier.com/locate/ijsolstr

Anti-plane shear Green's functions for an isotropic elastic half-space with a material surface

W.Q. Chen [a], Ch. Zhang [b,*]

[a] Department of Engineering Mechanics, Zhejiang University, Yuquan Campus, Hangzhou 310027, China
[b] Department of Civil Engineering, University of Siegen, D-57068 Siegen, Germany

ARTICLE INFO

Article history:
Received 12 February 2010
Received in revised form 5 March 2010
Available online 12 March 2010

Keywords:
Green's functions
Elastic half-space
Anti-plane shear
Surface elasticity

ABSTRACT

This paper presents analytical Green's function solutions for an isotropic elastic half-space subject to anti-plane shear deformation. The boundary of the half-space is modeled as a material surface, for which the Gurtin–Murdoch theory for surface elasticity is employed. By using Fourier cosine transform, analytical solutions for a point force applied both in the interior or on the boundary of the half-space are derived in terms of two particular integrals. Through simple numerical examples, it is shown that the surface elasticity has an important influence on the elastic field in the half-space. The present Green's functions can be used in boundary element method analysis of more complicated problems.

1. Introduction

The recent growing research interests in solid mechanics with the consideration of surface/interface effects have been inspired by the practical importance of particular micro- and nano-scaled phenomena in modern MEMS/NEMS technology. However, the surface/interface effects have already been noticed and studied for more than one hundred years (see Gibbs, 1961). The reader is referred to a review article by Cammarata (1994), which presented an in-depth discussion on some fundamental aspects and important issues of the surface/interface effects in thin films. In general, material scientists and physicists have paid much attention to these effects from the general thermodynamics considerations. Gurtin and Murdoch (1975), on the other hand, developed a rigorous mathematical framework for the continuum theory of a deformable material surface. It is shown that the conventional boundary conditions in classical elasticity are replaced by a set of two-dimensional differential equations governing the surface deformation. Based on their theory (hereafter, referred as the GM theory), Gurtin and Murdoch (1978) subsequently showed that the surface stress plays an important role in both the static and dynamical problems of elastic bodies with appropriate surfaces. It is interesting to point out that, through a particular procedure for developing plate theories, Mindlin (1963) was able to derive the approximate boundary conditions, which have exactly the same form as those in the GM theory except the coefficients when the residual surface tension is absent, on the plane boundary of a plate covered with a very thin layer. Based on the GM theory, a wide range of mechanics problems has been investigated in recent years, see He et al. (2004), Lim and He (2004), Lim et al. (2006), He and Li (2006), Li et al. (2006), Lü et al. (2009a,b), Ou et al. (2009) and Kim et al. (2010), to name a few.

As is well-known, Green's functions are very important in solving boundary-value problems in elasticity. Recently, there have appeared some studies on Green's functions for elastic bodies with surface effects. Based on the GM theory, but with a simplification that the surface material has the same elastic property as the bulk material, He and Lim (2006) presented the surface Green's function of a half-space using the double Fourier transforms; the interaction of a molecule with a half-space was studied using the derived surface Green's function. In their derivation, the incompressibility of the bulk material is also assumed. Wang and Feng (2007) reported analytical solutions of a half-plane with a material boundary subject to uniform as well as concentrated loads acting on the boundary. Fourier transform technique was used, and only the effect of residual surface tension was considered in their analysis. Their work was somewhat improved recently by Zhao and Rajapakse (2009), who considered the problem of a surface-loaded isotropic elastic layer with surface effects. Koguchi (2008) derived the surface Green's function for an anisotropic half-space with material surface using Stroh's formulism. However, his results are given in a very complicated integral form. No results of Green's functions for point loads applied in the bulk material have been reported, although they are more important and have wider applications in the boundary element analysis of more complicated problems.

* Corresponding author. Tel.: +49 271 7402173; fax: +49 271 7404074.
E-mail address: c.zhang@uni-siegen.de (Ch. Zhang).

0020-7683/$ - see front matter © 2010 Elsevier Ltd. All rights reserved.
doi:10.1016/j.ijsolstr.2010.03.007

In this paper, we confine ourselves to the simple anti-plane deformation of an isotropic elastic half-space subject to point shear force applied either in the bulk or on the surface. The plane boundary is modeled as a material surface which possesses both residual surface tension and elasticity, for which the GM theory is employed. Because of the symmetry of the problem, Fourier cosine transform is employed to derive the analytical expressions of the Green's functions. The properties of two specific integrals that seem to be closely associated with surface elasticity are summarized in an appendix of the paper. Numerical calculations are also performed to show the influence of surface elasticity on the stress field in the half-space.

2. Basic equations

The three-dimensional basic equations for the bulk material are conventional, and read as

$$\sigma_{ij,j} + f_i = 0 \tag{1}$$

$$\sigma_{ij} = \lambda \varepsilon_{kk}\delta_{ij} + 2\mu\varepsilon_{ij} \tag{2}$$

$$\varepsilon_{ij} = \frac{1}{2}(u_{i,j} + u_{j,i}) \tag{3}$$

where σ_{ij} and ε_{ij} are stress and strain tensors, respectively, u_i is the displacement vector, f_i is the body force vector, λ and μ are Lamé's constants, and δ_{ij} is the Kronecker delta. The convention of summation over repeated indices (with Latin indices running from 1 to 3, and Greek ones ranging over 1 and 2 only) is employed throughout this paper, and a comma followed by a subscript, say j, indicates differentiation with respect to the coordinate x_j in a Cartesian coordinate system.

For an infinite half-space $x_3 \geqslant 0$ as shown in Fig. 1, the equations governing the material surface $x_3 = 0$ are given by Gurtin and Murdoch (1978) as follows:

$$\sigma^s_{i\alpha,\alpha} + \sigma_{i3} = 0 \tag{4}$$

$$\sigma^s_{\alpha\beta} = \tau^s\delta_{\alpha\beta} + 2(\mu^s - \tau^s)\varepsilon_{\alpha\beta} + (\lambda^s + \tau^s)\varepsilon_{\gamma\gamma}\delta_{\alpha\beta} + \tau^s u_{\alpha,\beta} \tag{5}$$

$$\sigma^s_{3\beta} = \tau^s u_{3,\beta} \tag{6}$$

where the superscript s designates those quantities associated with the surface, τ^s is the residual surface tension, and λ^s and μ^s are the surface Lamé's moduli. In writing Eqs. (4)–(6), the displacement compatibility between the surface and bulk at $x_3 = 0$ has been implied.

In this paper, we confine ourselves to the simple case of anti-plane deformation of the half-space under an appropriate shear load, which is applied along and invariant with the x_2-direction (out of the figure). In this case, we have

$$u_1 = u_3 = 0, \quad u_2 = v(x_1, x_3) \tag{7}$$

Thus, for the bulk, we have only the following nonzero strain components:

$$\varepsilon_{12} = \frac{1}{2}\frac{\partial v}{\partial x_1}, \quad \varepsilon_{23} = \frac{1}{2}\frac{\partial v}{\partial x_3} \tag{8}$$

The nonzero stress components are obtained from the Hooke's law, Eq. (2), as

$$\sigma_{12} = \mu\frac{\partial v}{\partial x_1}, \quad \sigma_{23} = \mu\frac{\partial v}{\partial x_3} \tag{9}$$

The stress tensor in the bulk is symmetric, i.e. we have $\sigma_{12} = \sigma_{21}$ and $\sigma_{23} = \sigma_{32}$. The equilibrium equation (1) reduces to

$$\frac{\partial \sigma_{12}}{\partial x_1} + \frac{\partial \sigma_{23}}{\partial x_3} + f_2 = 0 \tag{10}$$

or in view of Eq. (9),

$$\frac{\partial^2 v}{\partial x_1^2} + \frac{\partial^2 v}{\partial x_3^2} + \frac{f_2}{\mu} = \nabla^2 v + \frac{f_2}{\mu} = 0 \tag{11}$$

where $\nabla^2 = \partial^2/\partial x_1^2 + \partial^2/\partial x_3^2$ is the two-dimensional Laplacian.

Accordingly, we have the following equations for the material surface $x_3 = 0$:

$$\frac{\partial \sigma^s_{21}}{\partial x_1} + \sigma_{23} = 0 \tag{12}$$

$$\sigma^s_{21} = \mu^s\frac{\partial v}{\partial x_1}, \quad \sigma^s_{12} = (\mu^s - \tau^s)\frac{\partial v}{\partial x_1} \tag{13}$$

Eq. (12) can also be obtained directly by invoking the equilibrium of an ultrathin film element (in the x_2-direction) as shown in Fig. 2, where σ_{23} is the 'external force' exerted by the underlying bulk material on the film. Eq. (4), which is for the general deformation cases, can be obtained with a similar consideration.

Note that for the complete theory developed by Gurtin and Murdoch (1975, 1978), the surface stress tensor $\sigma^s_{\alpha\beta}$ is not symmetric, i.e. $\sigma^s_{\alpha\beta} \neq \sigma^s_{\beta\alpha}$ when surface stress tension τ^s is present, as indicated clearly in Eq. (5).

For the current problem, the residual surface tension τ^s will contribute to the surface stress component σ^s_{12} only, and has entirely no effect on the elastic field in the interior of the half-space. This becomes obvious if we write the boundary conditions at $x_3 = 0$ as $\sigma_{23} = -\mu^s\partial^2 v/\partial x_1^2$, which is a straightforward result of Eqs. (12) and $(13)_1$.

For an external shear load $p(x_1, x_3)$ applied on the surface in the positive direction of x_2, Eq. (12) should be replaced by

$$\frac{\partial \sigma^s_{21}}{\partial x_1} + \sigma_{23} + p = 0 \tag{14}$$

which may also be obtained from the equilibrium consideration of the film element in Fig. 2.

3. Green's function solutions

3.1. Bulk Green's function

We first consider the case when a point shear force $f_3(x_1, x_3) = p_0\delta(x_1)\delta(x_3 - h)$ is applied in the interior of the

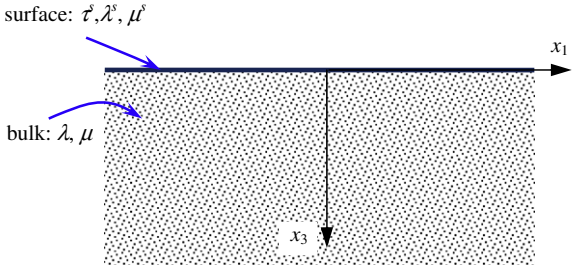

Fig. 1. A half-space $x_3 \geqslant 0$ with a material surface at $x_3 = 0$.

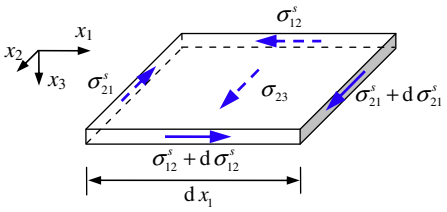

Fig. 2. The equilibrium of an ultrathin film element (the homogeneous residual stress state of $\sigma^s_{11} = \sigma^s_{22} = \tau^s$ is not shown).

half-space, here $h>0$ is the distance between the surface and the point at which the force is applied, see Fig. 3. Then, Eq. (11) reads

$$\frac{\partial^2 v}{\partial x_1^2}+\frac{\partial^2 v}{\partial x_3^2}+\frac{p_0}{\mu}\delta(x_1)\delta(x_3-h)=0 \tag{15}$$

The nontrivial homogeneous boundary conditions due to the presence of the material surface at $x_3=0$ are obtained, in view of Eq. (9), from Eqs. (12) and $(13)_1$ as

$$\mu^s\frac{\partial^2 v}{\partial x_1^2}+\mu\frac{\partial v}{\partial x_3}=0 \quad \text{at } x_3=0 \tag{16}$$

There are many ways to obtain the solution of Eq. (15) with the condition (16). We proceed to use the following Fourier cosine transform:

$$V(k;x_3)=\sqrt{\frac{2}{\pi}}\int_0^\infty v(x_1,x_3)\cos(kx_1)dx_1 \tag{17a}$$

$$v(x_1,x_3)=\sqrt{\frac{2}{\pi}}\int_0^\infty V(k;x_3)\cos(kx_1)dk \tag{17b}$$

And, instead of solving Eq. (15) directly, we divide the half-space into two regions, region 1 ($0\leqslant x_3\leqslant h$) and region 2 ($x_3\geqslant h$), as shown in Fig. 3. By doing so, the governing equation in each region becomes homogeneous as

$$\frac{\partial^2 v^{(\kappa)}}{\partial x_1^2}+\frac{\partial^2 v^{(\kappa)}}{\partial x_3^2}=0 \quad (\kappa=1,2) \tag{18}$$

while at $x_3=h$, we have the following continuity/equilibrium conditions:

$$v^{(1)}=v^{(2)}, \quad \mu\frac{\partial v^{(2)}}{\partial x_3}+p_0\delta(x_1)=\mu\frac{\partial v^{(1)}}{\partial x_3} \tag{19}$$

where the superscript κ denotes the respective region. The condition at $x_3=0$ is still given by Eq. (16), but with v replaced by $v^{(1)}$.

Now, by applying the cosine Fourier transform defined by Eq. (17a) to Eq. (18) and conditions (16) and (19), we get

$$\frac{d^2V^{(\kappa)}}{dx_3^2}-k^2V^{(\kappa)}=0 \quad (\kappa=1,2) \tag{20}$$

$$\frac{dV^{(1)}}{dx_3}-r_\mu k^2V^{(1)}=0 \quad \text{at } x_3=0 \tag{21}$$

$$V^{(1)}=V^{(2)}, \quad \frac{dV^{(2)}}{dx_3}+\frac{p_0}{\mu}\frac{1}{\sqrt{2\pi}}=\frac{dV^{(1)}}{dx_3} \tag{22}$$

where $r_\mu=\mu^s/\mu$ is the shear modulus ratio between the surface and bulk, and it has the dimension of length, which can be regarded as an intrinsic length parameter of the half-space with a material boundary.

Taking into account the regularity condition at $x_3\to\infty$, we can write down the solutions to Eq. (20) in the two regions as

$$V^{(1)}=A^{(1)}e^{kx_3}+B^{(1)}e^{-kx_3}, \quad V^{(2)}=B^{(2)}e^{-kx_3} \tag{23}$$

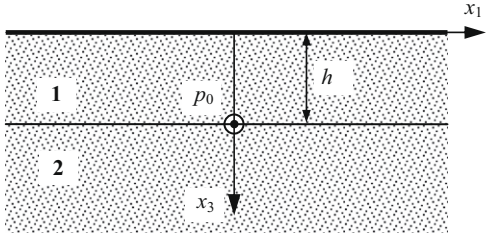

Fig. 3. A point shear force p_0 acting in the bulk at point $(0,h)$.

Substituting into Eqs. (21) and (22) yields

$$\begin{aligned}
&A^{(1)}k-B^{(1)}k-r_\mu k^2(A^{(1)}+B^{(1)})=0\\
&A^{(1)}e^{kh}+B^{(1)}e^{-kh}-B^{(2)}e^{-kh}=0\\
&A^{(1)}ke^{kh}-B^{(1)}ke^{-kh}+B^{(2)}ke^{-kh}=\frac{p_0}{\mu}\frac{1}{\sqrt{2\pi}}
\end{aligned} \tag{24}$$

Thus, we can obtain

$$\begin{aligned}
A^{(1)}&=\frac{e^{-kh}}{k}\frac{1}{2\sqrt{2\pi}}\frac{p_0}{\mu}\\
B^{(1)}&=\frac{(1-r_\mu k)e^{-kh}}{k(1+r_\mu k)}\frac{1}{2\sqrt{2\pi}}\frac{p_0}{\mu}\\
B^{(2)}&=\frac{1}{k}\left[e^{kh}+\frac{(1-r_\mu k)}{(1+r_\mu k)}e^{-kh}\right]\frac{1}{2\sqrt{2\pi}}\frac{p_0}{\mu}
\end{aligned} \tag{25}$$

Substituting into Eq. (23) and then performing the inverse transform, we get

$$v^{(1)}=\frac{1}{2\pi}\frac{p_0}{\mu}\int_0^\infty\left[\frac{1}{k}e^{-k(h-x_3)}+\frac{(1-r_\mu k)}{k(1+r_\mu k)}e^{-k(h+x_3)}\right]\cos(kx_1)dk \tag{26a}$$

$$=\frac{1}{4\pi}\frac{p_0}{\mu}\ln\left[\frac{x_1^2+(h+x_3)^2}{x_1^2+(h-x_3)^2}\right]+\frac{1}{\pi}\frac{p_0}{\mu}[I_c(x_1,h+x_3)-J_c(x_1,h+x_3;r_\mu)] \tag{26b}$$

$$v^{(2)}=\frac{1}{2\pi}\frac{p_0}{\mu}\int_0^\infty\frac{1}{k}\left[e^{-k(x_3-h)}+\frac{(1-r_\mu k)}{(1+r_\mu k)}e^{-k(x_3+h)}\right]\cos(kx_1)dk \tag{26c}$$

$$=\frac{1}{4\pi}\frac{p_0}{\mu}\ln\left[\frac{x_1^2+(x_3+h)^2}{x_1^2+(x_3-h)^2}\right]+\frac{1}{\pi}\frac{p_0}{\mu}[I_c(x_1,x_3+h)-J_c(x_1,x_3+h;r_\mu)] \tag{26d}$$

where

$$I_c(x,y)=\int_0^\infty\frac{e^{-ky}}{k}\cos(kx)dk=-\gamma-\frac{1}{2}\ln(x^2+y^2),$$

$$J_c(x,y;a)=\int_0^\infty\frac{ae^{-ky}}{1+ak}\cos(kx)dk$$

with $\gamma=0.57721\ldots$ being the Euler constant. It is noted that the second integral can be expressed in terms of the well-known exponential integral, see Appendix A.

It is noted that the Euler constant, which corresponds to a rigid-body translation, can be eliminated since it does not affect the stress and strain fields in the half-space. Moreover, we note that the two expressions for v, as given in Eqs. (26b) and (26d) respectively, are identical, and hence the displacement in the half-space can be simply written as

$$\begin{aligned}
v=&-\frac{1}{4\pi}\frac{p_0}{\mu}\ln\left\{[x_1^2+(x_3-h)^2][x_1^2+(x_3+h)^2]\right\}\\
&-\frac{1}{\pi}\frac{p_0}{\mu}J_c(x_1,x_3+h;r_\mu)
\end{aligned} \tag{27}$$

where the constant term corresponding to the rigid-body translation has been omitted.

The shear stresses in the half-space then can be obtained from Eqs. (9) and (27) as

$$\sigma_{12}=-\frac{p_0}{\pi}\left\{\frac{2x_1x_3h}{[x_1^2+(x_3-h)^2][x_1^2+(x_3+h)^2]}+\frac{1}{r_\mu}J_s(x_1,x_3+h;r_\mu)\right\} \tag{28}$$

$$\sigma_{23}=-\frac{p_0}{\pi}\left\{\frac{(x_3^2-x_1^2-h^2)h}{[x_1^2+(x_3-h)^2][x_1^2+(x_3+h)^2]}+\frac{1}{r_\mu}J_c(x_1,x_3+h;r_\mu)\right\} \tag{29}$$

where

$$J_s(x,y;a)=\int_0^\infty\frac{ae^{-ky}}{1+ak}\sin(kx)dk$$

and the equalities in Eq. (A6) in Appendix A have been employed in deriving Eqs. (28) and (29).

The surface stress components can also be calculated from Eqs. (13) and (27) as

$$\sigma_{21}^s = -\frac{p_0}{\pi} J_s(x_1, h; r_\mu), \quad \sigma_{12}^s = -\frac{(\mu^s - \tau^s)}{\mu^s} \frac{p_0}{\pi} J_s(x_1, h; r_\mu) \tag{30}$$

If the surface elasticity is absent, then the classical results of the half-space subject to a point shear load are obtained as follows:

$$v = -\frac{1}{4\pi} \frac{p_0}{\mu} \ln\{[x_1^2 + (x_3 - h)^2][x_1^2 + (x_3 + h)^2]\} \tag{31}$$

$$\sigma_{12} = -\frac{p_0}{\pi} \frac{x_1(x_1^2 + x_3^2 + h^2)}{[x_1^2 + (x_3 - h)^2][x_1^2 + (x_3 + h)^2]} \tag{32}$$

$$\sigma_{23} = -\frac{p_0}{\pi} \frac{x_3(x_1^2 + x_3^2 - h^2)}{[x_1^2 + (x_3 - h)^2][x_1^2 + (x_3 + h)^2]} \tag{33}$$

It is readily seen that the expression in Eq. (31) agrees with the result of the two-dimensional anti-plane (potential) problem of a half-space (Gaul et al., 2003), as it should be.

For a unit point load applied at an arbitrary interior point (x_1', x_3'), Eq. (15) becomes

$$\frac{\partial^2 v^*}{\partial x_1^2} + \frac{\partial^2 v^*}{\partial x_3^2} + \frac{1}{\mu}\delta(x_1 - x_1')\delta(x_3 - x_3') = 0 \tag{34}$$

where the superscript * indicates the point-source Green's function solution. Then the expression for displacement can be given in a standard form of Green's functions as

$$v^*(\mathbf{x}, \mathbf{x}') = -\frac{1}{2\pi\mu}(\ln r + \ln R) - \frac{1}{\pi\mu} J_c(x_1 - x_1', x_3 + x_3'; r_\mu) \tag{35}$$

where $\mathbf{x}$ and $\mathbf{x}'$ denote the position vectors of the field point (x_1, x_3) and the source point (x_1', x_3'), respectively, $r = |\mathbf{x} - \mathbf{x}'| = \sqrt{(x_1 - x_1')^2 + (x_3 - x_3')^2}$ is the distance between $\mathbf{x}$ and $\mathbf{x}'$, and $R = \sqrt{(x_1 - x_1')^2 + (x_3 + x_3')^2}$ is the distance between $\mathbf{x}$ and the imagine of $\mathbf{x}'$. The first term in v^* contains a logarithmic singularity (weak singularity) as that for the potential problem of an infinite plane subject to a point source, the second term is due to the presence of the plane boundary $x_3 = 0$ and has no singularity since $x_3' > 0$ (i.e. the load is applied in the interior of the half-plane), and the third is caused by the surface elasticity, which is also nonsingular as can be seen from the discussions presented in Appendix A.

Because of the symmetry property of the integral J_c as indicated in Eq. (A3), we know that $v^*(\mathbf{x}, \mathbf{x}') = v^*(\mathbf{x}', \mathbf{x})$, which indicates that the reciprocity theorem still works for a body with material surface as considered here.

In accordance with Eq. (35), the stress Green's functions can be written as

$$\sigma_{12}^*(\mathbf{x}, \mathbf{x}') = -\frac{1}{2\pi}\left(\frac{x_1 - x_1'}{r^2} - \frac{x_1 - x_1'}{R^2}\right) - \frac{1}{\pi}\frac{1}{r_\mu} J_s(x_1 - x_1', x_3 + x_3'; r_\mu) \tag{36a}$$

$$\sigma_{23}^*(\mathbf{x}, \mathbf{x}') = -\frac{1}{2\pi}\left(\frac{x_3 - x_3'}{r^2} - \frac{x_3 + x_3'}{R^2}\right) - \frac{1}{\pi}\frac{1}{r_\mu} J_c(x_1 - x_1', x_3 + x_3'; r_\mu) \tag{36b}$$

It is seen that both stress components have the same strong singularity $(x_i - x_i')/r^2$ as in the conventional potential problems (Brebbia and Walker, 1979; Gaul et al., 2003). The above-mentioned singularity characteristics of the displacement and stress Green's functions have an important implication in constructing the corresponding boundary integral equation, and will be briefly discussed in Appendix B.

3.2. Surface Green's function

In the case that the point shear force $p(x_1, x_3) = p_0\delta(x_1)\delta(x_3)$ is applied on the surface, we need not divide the bulk into two regions, and the governing equations and boundary conditions are, respectively

$$\frac{\partial^2 v}{\partial x_1^2} + \frac{\partial^2 v}{\partial x_3^2} = 0 \quad (x_3 > 0) \tag{37}$$

$$\mu^s \frac{\partial^2 v}{\partial x_1^2} + \mu \frac{\partial v}{\partial x_3} = -p_0\delta(x_1) \quad \text{at } x_3 = 0 \tag{38}$$

The corresponding Fourier transforms are

$$\frac{d^2 V}{dx_3^2} - k^2 V = 0 \quad (x_3 > 0) \tag{39}$$

$$\frac{dV}{dx_3} - r_\mu k^2 V = -\frac{p_0}{\mu}\frac{1}{\sqrt{2\pi}} \quad \text{at } x_3 = 0 \tag{40}$$

The solution of Eq. (37), which satisfies the regularity condition at $x_3 \to \infty$ is

$$V = Be^{-kx_3} \tag{41}$$

Then from Eq. (40), we get

$$B = \frac{1}{k(1 + r_\mu k)} \frac{p_0}{\mu} \frac{1}{\sqrt{2\pi}} \tag{42}$$

And the displacement can be obtained as

$$\begin{aligned} v &= \frac{1}{\pi}\frac{p_0}{\mu}\int_0^\infty \frac{1}{k(1 + r_\mu k)} e^{-kx_3}\cos(kx_1)dk \\ &= \frac{1}{\pi}\frac{p_0}{\mu}[I_c(x_1, x_3) - J_c(x_1, x_3; r_\mu)] \end{aligned} \tag{43}$$

By eliminating the constant term, we obtain

$$v = -\frac{1}{2\pi}\frac{p_0}{\mu}\ln(x_1^2 + x_3^2) - \frac{1}{\pi}\frac{p_0}{\mu} J_c(x_1, x_3; r_\mu) \tag{44}$$

which can be directly derived from Eq. (27) by making the substitution $h = 0$. The shear stress components in the bulk are calculated as

$$\sigma_{12} = -\frac{p_0}{r_\mu \pi} J_s(x_1, x_3; r_\mu), \quad \sigma_{23} = -\frac{p_0}{r_\mu \pi} J_c(x_1, x_3; r_\mu) \tag{45}$$

and those of the material surface are

$$\sigma_{21}^s = -\frac{p_0}{\pi} J_s(x_1, 0; r_\mu), \quad \sigma_{12}^s = -\frac{(\mu^s - \tau^s)}{\mu^s}\frac{p_0}{\pi} J_s(x_1, 0; r_\mu) \tag{46}$$

If the surface elasticity is absent, we then have the following classical results:

$$v = -\frac{1}{2\pi}\frac{p_0}{\mu}\ln(x_1^2 + x_3^2) \tag{47}$$

$$\sigma_{12} = -\frac{p_0}{\pi}\frac{x_1}{x_1^2 + x_3^2}, \quad \sigma_{23} = -\frac{p_0}{\pi}\frac{x_3}{x_1^2 + x_3^2} \tag{48}$$

As noticed above, the surface Green's function of an elastic half-space with a material surface can be obtained from the bulk Green's function by simply letting $h = 0$, just as in the classical elasticity. In other words, the presence of surface elasticity does not alter the nature of such a limiting procedure. Thus, in most applications it seems not necessary to distinguish these two cases particularly. One exception is the singular behavior of the surface stress Green's function, which is different from that for the bulk stress Green's function, as clearly shown by Eq. (45). This point will be further discussed in the next section along with the numerical demonstration. The change of the singular behavior of the surface stress Green's function will not affect the associated BEM formulation except one coefficient, as discussed in Appendix B.

4. Numerical results

For numerical calculations and comparison, we introduce the following dimensionless quantities:

$$\hat{\sigma}_{12}=\frac{\sigma_{12}\pi r_\mu}{p_0},\quad \hat{\sigma}_{23}=\frac{\sigma_{23}\pi r_\mu}{p_0},\quad x=\frac{x_1}{r_\mu},\quad y=\frac{x_3}{r_\mu},\quad \hat{h}=\frac{h}{r_\mu} \tag{49}$$

Figs. 4 and 5 depict the distributions of dimensionless bulk stress components $\hat{\sigma}_{12}$ and $\hat{\sigma}_{23}$, respectively, for various values of the dimensionless depth y along the horizontal axis . The location of the load is specified as $\hat{h}=0.1$. It is noted that, by using the dimensionless quantities defined in Eq. (49), it is not necessary to assign any particular value to the parameter r_μ since, as an intrinsic length, it has been used to eliminate the length dimension. Actually, it can be easily found from the dimensionless form of Eqs. (28) and (29) that, the dimensionless stresses $\hat{\sigma}_{12}$ and $\hat{\sigma}_{23}$ no longer depend apparently on r_μ. Thus, the difference in r_μ will have completely no influence on Figs. 4 and 5. For comparison, the predictions corresponding to the classical solution without any surface effect are also given in the figures, which are indicated by CS, while those with surface effect are indicated by SE. As we can see, the surface elasticity has a more significant effect on the stresses near the surface of the half-space than those far from the surface. Furthermore, the presence of the surface elasticity seems to lower the shear stress $\hat{\sigma}_{12}$, especially at the locations near the material surface. For the shear stress $\hat{\sigma}_{23}$, while the classical solution correctly gives the traction-free boundary conditions ($\sigma_{23}=0$) at $x_3=0$, the solution with surface effect is not trivial, and its maximum positive value appears at $x_1=0$. Furthermore, we can see that surface elasticity may alter the nature of the shear stress $\hat{\sigma}_{23}$, i.e. a negative $\hat{\sigma}_{23}$ at a certain point in the classical elasticity may be changed to a positive one due to the surface effect.

Miller and Shenoy (2000) have computed from empirical atomic potentials the bulk and surface elastic properties of FCC Al and diamond Si, both having cubic symmetry. According to their results, for similar isotropic materials, the values of τ^s/μ and μ^s/μ can be estimated as 0.1 Å and 1.0 Å, respectively (He and Li, 2006). Thus, the intrinsic length of the problem can be taken as $r_\mu=1.0$ Å. If this is the case, then the value of $\hat{h}=0.1$ means that $h=0.1$ Å. This value is very small, but the results given in Figs. 4 and 5 still serve an illustrative purpose since, as mentioned earlier, the intrinsic length parameter r_μ has no influence on the results. To make it clearer, let's take a different value of h, say 10 Å. Then to keep $\hat{h}$ unchanged (i.e. $\hat{h}=0.1$), we can artificially assume $r_\mu=100$ Å. The dimensionless results will be still given by Figs. 4 and 5, but the real stress field in the half-space changes. The magnitude of stresses (σ_{12} and σ_{23}) will become one hundred times as small as those for $h=0.1$ Å at a point with both coordinates amplified by one hundred times. Thus, quite similar observations can be obtained for larger values of h, except the difference in magnitudes of the real stress field. The intrinsic parameter r_μ, acting a role of zooming in/out or simply scaling, is hence very important in interpreting the stress and displacement distributions in the half-space with a material surface.

When the load is applied on the surface, the distributions of $\hat{\sigma}_{12}$ and $\hat{\sigma}_{23}$ are shown in Figs. 6 and 7, respectively. By comparing Fig. 6 with Fig. 4, a notable difference is found that the shear stress σ_{12} is no longer singular at the load application point when the surface effect is taken into consideration, as can be seen clearly from Eq. (45). Obviously, it is due to the mutual cancellation of the two

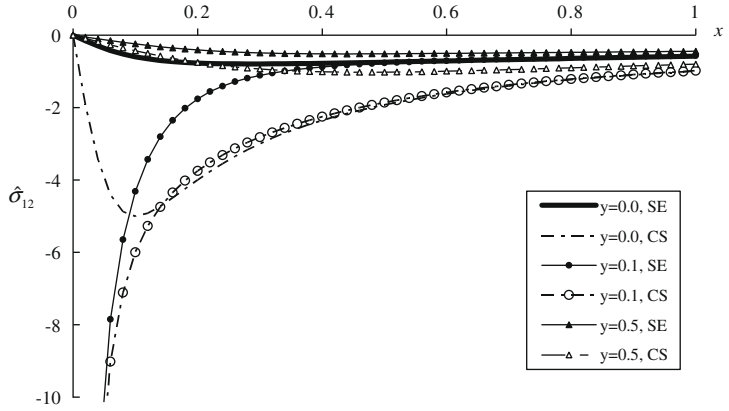

Fig. 4. Distributions of dimensionless shear stress component $\hat{\sigma}_{12}=\sigma_{12}\pi r_\mu/p_0$ at various depths $x_3=yr_\mu$ along the horizontal axis $x_1=xr_\mu$ for $\hat{h}=h/r_\mu=0.1$; SE denotes the solution including the surface effect, and CS corresponds to the classical elasticity.

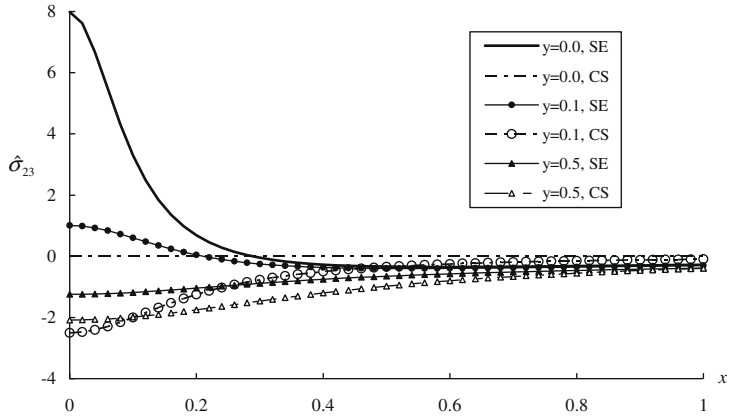

Fig. 5. Distributions of dimensionless shear stress component $\hat{\sigma}_{23}=\sigma_{23}\pi r_\mu/p_0$ at various depths $x_3=yr_\mu$ along the horizontal axis $x_1=xr_\mu$ for $\hat{h}=h/r_\mu=0.1$; SE denotes the solution including the surface effect, and CS corresponds to the classical elasticity.

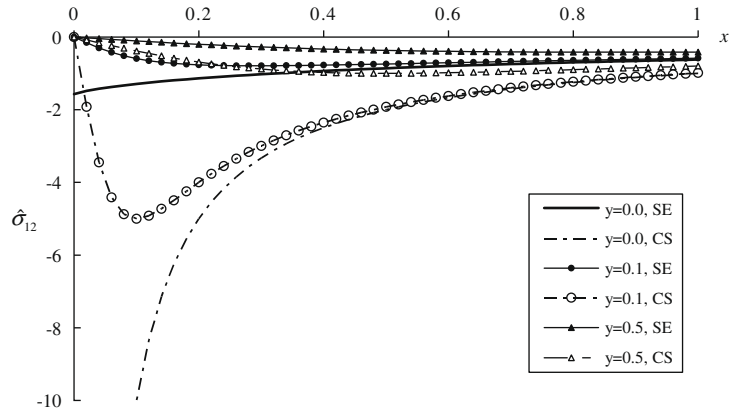

Fig. 6. Distributions of dimensionless shear stress component $\hat{\sigma}_{12} = \sigma_{12}\pi r_\mu/p_0$ at various depths $x_3 = yr_\mu$ along the horizontal axis $x_1 = xr_\mu$ for $\hat{h} = h/r_\mu = 0.0$; SE denotes the solution including the surface effect, and CS corresponds to the classical elasticity.

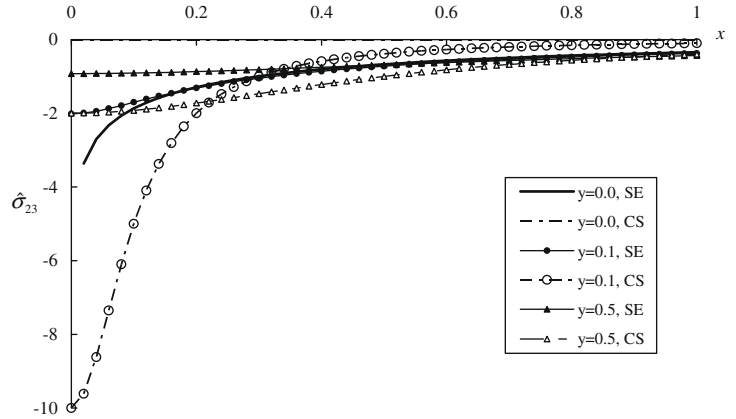

Fig. 7. Distributions of dimensionless shear stress component $\hat{\sigma}_{23} = \sigma_{23}\pi r_\mu/p_0$ at various depths $x_3 = yr_\mu$ along the horizontal axis $x_1 = xr_\mu$ for $\hat{h} = h/r_\mu = 0.0$; SE denotes the solution including the surface effect, and CS corresponds to the classical elasticity.

singular terms, one corresponding to the classical elasticity and another induced by the surface elasticity. Although this is a very interesting phenomenon, it is not a universal conclusion that can be applied to all stress components. In fact, the shear stress component σ_{23} is still singular (of logarithmic type) at the load point, as can be seen from Eqs. (45) and (A11). In the classical elasticity theory, σ_{23} vanishes identically when $x_3 = 0$ except at the load point (0,0); while in the present theory with a surface elasticity, it has a finite value and varies with x_1, except at the load point (0,0) where it is also infinite.

To characterize the range of the influence of surface elasticity on the stress field, we show in Fig. 8 the spatial distribution of the stress ratio $\varpi = \sigma_{23}^{SE}/\sigma_{23}^{CS}$, where the superscripts *SE* and *CS* denote the solution involving surface effect and the classical solution, respectively. The load is assumed to be on the surface, i.e. $h = 0$. As can be seen from the figure, when $y = 25$, i.e. at the depth of 25 times the intrinsic length, the relative difference between the two solutions becomes smaller than 5%. This is also the case for the shear stress component σ_{12} (although not shown here), and hence the surface elasticity can be regarded to have an influence on the stress field in the range within the depth of 25 times the intrinsic length. As expected, if the intrinsic length reduces, then the influence range also shrinks. If the load is not applied on the surface, the spatial distribution of $\varpi = \sigma_{23}^{SE}/\sigma_{23}^{CS}$ is very similar, see Fig. 9 for $\hat{h} = 0.1$ (for other load positions, the scaling argument mentioned earlier may be used to obtain the influence range).

From its expression in Eq. (28), it is known that the stress σ_{12} is antisymmetric with respect to the vertical axis $x_1 = 0$, and hence vanishes there except at the load point. On the other hand, as seen from Eq. (29), the stress σ_{23} is symmetric with respect to the vertical axis, and does not vanish at $x_1 = 0$. Fig. 10 displays the distributions of $\hat{\sigma}_{23}$ along the vertical axis for various positions of the load. The singularity at the load point is clearly shown. It is also seen that the bulk stress on the boundary increases when the load approaches to the surface.

To show the effect of the surface elasticity on the displacement, we define the dimensionless displacement difference $\hat{v}_d$ as

$$\hat{v}_d = \frac{\pi\mu}{p_0}(v^{CS} - v^{SE}) = J_c(x_1, x_3 + h; r_\mu) \tag{50}$$

The characteristics of the integral J_c are discussed in Appendix A and its drawings are given in Fig. A1. If the load is applied on the surface, then Fig. A1 gives $\hat{v}_d$ at various depths $y = 0, 1, 2$ and 4. It is seen that the displacement difference at $x_3 = 0$ is not always larger than those underneath the boundary. Only near the load application point, where it is singular, it is the largest, while with the increase of distance away from the load, it becomes smaller and smaller. Actually, beyond approximately $x = 2$, it becomes the lowest one among the four curves. If the load is applied at $(0, r_\mu)$, then the curve $y = 1$ in Fig. A1 corresponds to $\hat{v}_d$ at the boundary, and $y = 2$ gives the results for $x_3 = r_\mu$. As can be seen clearly, there is no singularity at the load point. The displacement difference also decreases with

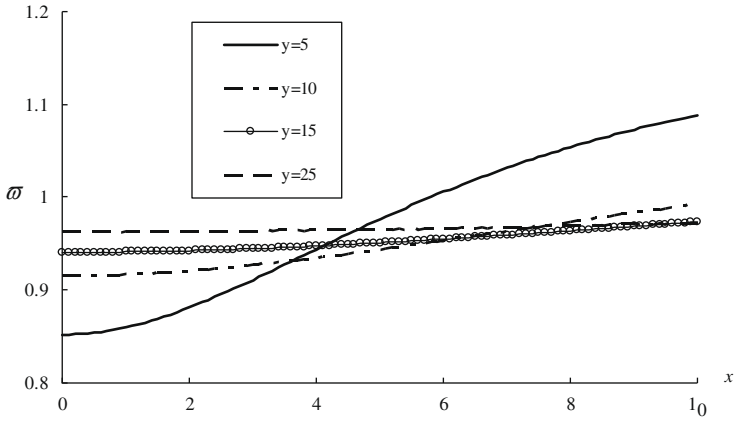

Fig. 8. Distributions of stress ratio $\varpi = \sigma_{23}^{SE}/\sigma_{23}^{CS}$ at various depths $x_3 = yr_\mu$ along the horizontal axis $x_1 = xr_\mu$ for $\hat{h} = h/r_\mu = 0.0$.

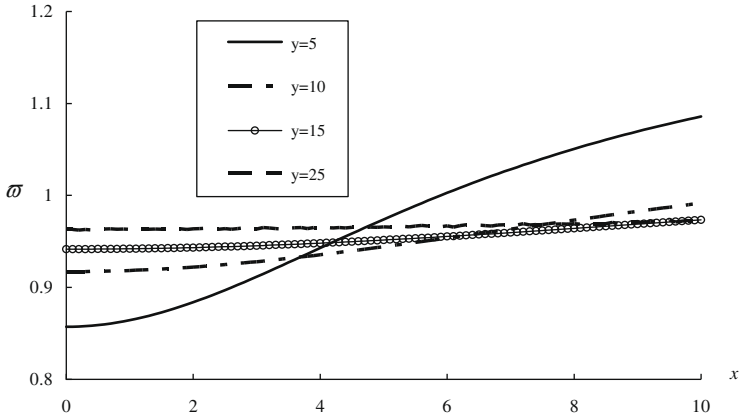

Fig. 9. Distributions of stress ratio $\varpi = \sigma_{23}^{SE}/\sigma_{23}^{CS}$ at various depths $x_3 = yr_\mu$ along the horizontal axis $x_1 = xr_\mu$ for $\hat{h} = h/r_\mu = 0.1$.

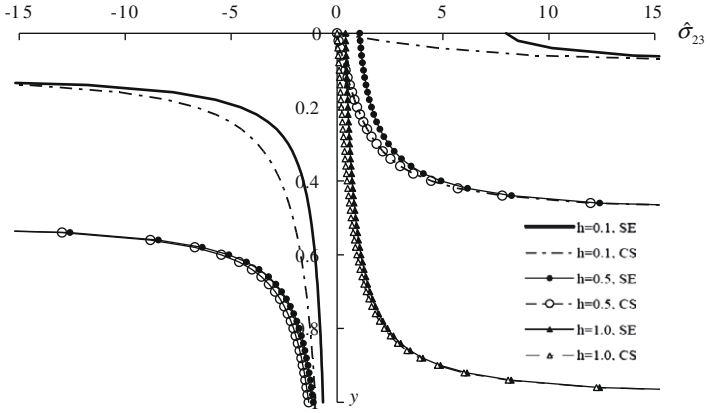

Fig. 10. Distributions of $\hat{\sigma}_{23} = \sigma_{23}\pi r_\mu/p_0$ along the vertical axis $x_3 = yr_\mu$ for $\hat{h} = h/r_\mu = 0.1, 0.5$ and 1.0; SE denotes the solution including the surface effect, and CS corresponds to the classical elasticity.

the distance away from the load point. A typical two-dimensional distribution of $\hat{v}_d$ is given in Fig. 11 for $\hat{h} = 0.1$.

5. Conclusions

Analytical Green's functions have been obtained for an isotropic elastic half-space subject to a point force loading under the assumption of anti-plane shear deformation. The Gurtin–Murdoch continuum theory has been adopted to describe the deformation of the plane boundary surface, which may have different elastic property from the bulk material. Fourier cosine transform technique is used to derive the analytical expressions of the Green's functions, in which two particular integrals are involved and studied. Numerical examples show that the surface effect has an important influence on the elastic field in the half-space.

The present Green's functions are useful in order to obtain numerical solutions for more complicated problems for which the boundary element method (BEM) may be employed (Telles

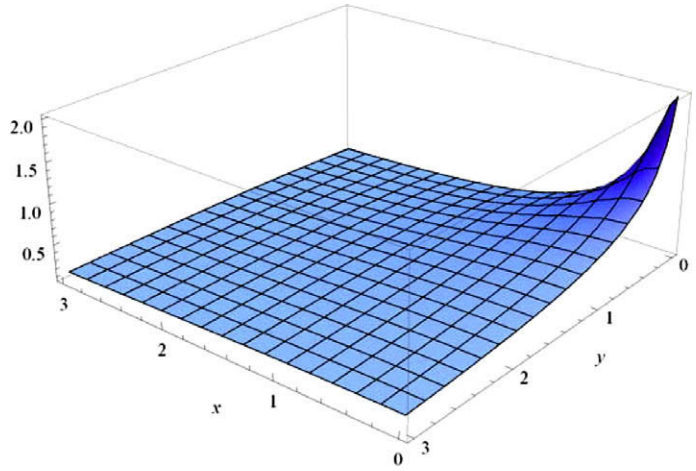

Fig. 11. The two-dimensional distribution of $\hat{v}_d$, which is defined in Eq. (50), for $\hat{h} = h/r_\mu = 0.1$.

and Brebbia, 1981). The corresponding boundary integral equation formulation is presented in Appendix B. An in-depth discussion on BEM is however beyond the scope of this paper and will be given elsewhere.

Acknowledgements

The work was sponsored by the National Natural Science Foundation of China (Nos. 10725210 and 10832009). Financial support from the German Research Foundation (DFG, Project-No. ZH 15/15-1) is also acknowledged.

Appendix A. Some properties of the integrals $J_c(x,y;a)$ and $J_s(x,y;a)$

The following two integral functions are defined in the text:

$$J_c(x,y;a) = \int_0^\infty \frac{ae^{-ky}}{1+ak}\cos(kx)dk$$
$$J_s(x,y;a) = \int_0^\infty \frac{ae^{-ky}}{1+ak}\sin(kx)dk \tag{A1}$$

where, according to the physical problem, we confine ourselves to the case x, y, a are all real and $\geqslant 0$. It seems that these two integrals will be present in the solutions of some problems involving the surface effect, see Zhao and Rajapakse (2009) for example, although their definition is slightly different from ours. Hence the properties of the two integrals deserve a little deeper investigation. In the following, we only list some primary properties.

An immediate result of Eq. (A1) is as follows:

$$J_c(x,y;a) = J_c(x/a,y/a;1), \quad J_s(x,y;a) = J_s(x/a,y/a;1) \tag{A2}$$

which indicates the inherent scaling function of the parameter a in the two integrals. This scaling property exactly accords with the physical nature arising in the current problem. Note that if $a = 0$, both integrals vanish.

The following symmetry property is also obvious:

$$J_c(x,y;a) = J_c(-x,y;a), \quad J_s(x,y;a) = -J_s(-x,y;a) \tag{A3}$$

which reveals the symmetry of the Green's function with respect to the source point and the field point, as already noticed in the text.

Since

$$J_c(x,y;a) - iJ_s(x,y;a) = \int_0^\infty \frac{ae^{-k(y+ix)}}{1+ak}dk = \int_0^\infty \frac{e^{-\xi z}}{1+\xi}d\xi \tag{A4}$$

where $z = (y+ix)/a$, we then, through simple variable substitution, obtain the following relations:

$$J_c(x,y;a) = \mathrm{Re}[e^z E_1(z)] = \frac{1}{2}[e^z E_1(z) + e^{\bar{z}} E_1(\bar{z})]$$
$$J_s(x,y;a) = -\mathrm{Im}[e^z E_1(z)] = \frac{i}{2}[e^z E_1(z) - e^{\bar{z}} E_1(\bar{z})] \tag{A5}$$

and

$$E_1(z) = \int_z^\infty (e^{-t}/t)dt \quad (|Arg(z)| < \pi)$$

being the exponential integral (Abramovitz and Stegun, 1964).

Further, it can be shown that

$$\frac{\partial J_c(x,y;a)}{\partial x} = -\frac{x}{x^2+y^2} + \frac{1}{a}J_s(x,y;a)$$
$$\frac{\partial J_c(x,y;a)}{\partial y} = -\frac{y}{x^2+y^2} + \frac{1}{a}J_c(x,y;a) \tag{A6}$$

$$\frac{\partial J_s(x,y;a)}{\partial x} = \frac{y}{x^2+y^2} - \frac{1}{a}J_c(x,y;a)$$
$$\frac{\partial J_s(x,y;a)}{\partial y} = -\frac{x}{x^2+y^2} + \frac{1}{a}J_s(x,y;a) \tag{A7}$$

This differential property is particular useful in obtaining the stress fields for related problems, as shown in the text as well as in Zhao and Rajapakse (2009). We also notice from Eqs. (A6) and (A7) that

$$\frac{\partial J_c(x,y;a)}{\partial x} = \frac{\partial J_s(x,y;a)}{\partial y}, \quad \frac{\partial J_c(x,y;a)}{\partial y} = -\frac{\partial J_s(x,y;a)}{\partial x} \tag{A8}$$

It is also interesting to study some particular cases when x or y is known. First, let us assume $x = 0$, for which Eq. (A1) becomes

$$J_c(0,y;a) = \int_0^\infty \frac{ae^{-ky}}{1+ak}dk = e^{y/a}E_1(y/a) = e^{y/a}\Gamma(0,y/a) \tag{A9}$$
$$J_s(0,y;a) = 0 \ \ (y \neq 0), \quad J_s(0,0;a) = \pi/2 \tag{A10}$$

where $\Gamma(m,z) = \int_z^\infty t^{m-1}e^{-t}dt$ is the incomplete Gamma function. It is then easy to see that

$$\lim_{y\to 0} J_c(0,y;a) = -\lim_{y\to 0}\ln(y/a) = \infty \quad (a \neq 0) \tag{A11}$$

Thus the term due to the surface elasticity in Eq. (27) exhibits a logarithmic singularity at the load application point only when it is on the surface since in the solution we have $y = x_3 + h$. Such a singularity is expected since the material surface can be regarded as a very thin layer of elastic material. Nevertheless, when the load is applied

on the surface, the displacement still exhibits a logarithmic singularity at the load application point. However, the singular behavior of the stress field will change, as discussed in the numerical example in Section 4.

On the other hand, by taking $y = 0$, we obtain

$$J_c(x,0;a) = \int_0^\infty \frac{a\cos(kx)}{1+ak}dk = g(x/a)$$
$$J_s(x,0;a) = \int_0^\infty \frac{a\sin(kx)}{1+ak}dk = f(x/a) \tag{A12}$$

where $f(z) = \int_0^\infty [\sin(t)/(t+z)]dt$ and $g(z) = \int_0^\infty [\cos(t)/(t+z)]dt$ are auxiliary functions defined in Abramovitz and Stegun (1964). They are related to the well-known sine and cosine integrals by

$$f(z) = Ci(z)\sin(z) - si(z)\cos(z)$$
$$g(z) = -Ci(z)\cos(z) - si(z)\sin(z) \tag{A13}$$

with $si(z) = Si(z) - \pi/2$ and

$$Si(z) = \int_0^z \frac{\sin(t)}{t}dt$$
$$Ci(z) = -\int_z^\infty \frac{\cos(t)}{t}dt \quad (|Arg(z)| < \pi) \tag{A14}$$

being the sine and cosine integrals. The fact that $f(0) = \pi/2$ results in $J_s(0,0;a) = \pi/2$ as already given in Eq. (A10).

To gain a direct knowledge of their behavior, we show in Figs. A1 and A2 the drawings of the two integral functions, respectively. They are depicted at $a = 1$, while those for $a \neq 1$ can be easily imaged based on the scaling property mentioned above.

Appendix B. Boundary integral equation formulation for an isotropic elastic half-space with a material surface

If in the interior of the half-space there contains additional internal boundaries caused by cracks, holes or inclusions, then the displacement and stress fields may be very difficult to obtain analytically. In such cases, an approximate solution may be sought for by the boundary element method (BEM), which is based on the boundary integral equation (Brebbia and Walker, 1979). The Green's functions obtained in the text then play a central role in constructing such a formulation, as shown below.

We start from the following two-dimensional Green's second identity

$$\int_A (v\nabla^2 v^* - v^*\nabla^2 v)dA = \int_L \left(v\frac{\partial v^*}{\partial n} - v^*\frac{\partial v}{\partial n}\right)dL \tag{B1}$$

where v is the displacement field for a particular problem, v^* is the displacement Green's function given in Eq. (35), A is the area occupied by the elastic body with the boundary L, and $\mathbf{n}$ is the outward pointing unit normal.

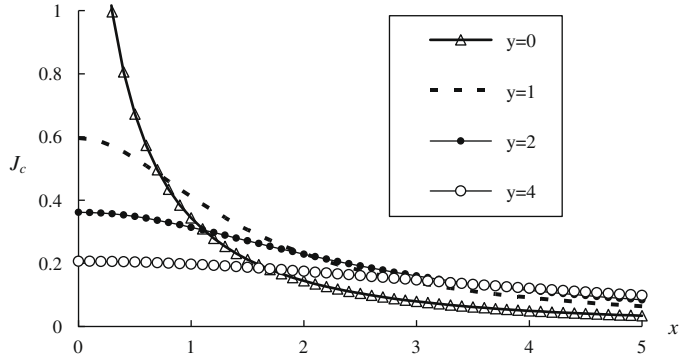

Fig. A1. Integral $J_c(x,y;a)$ for $a = 1$.

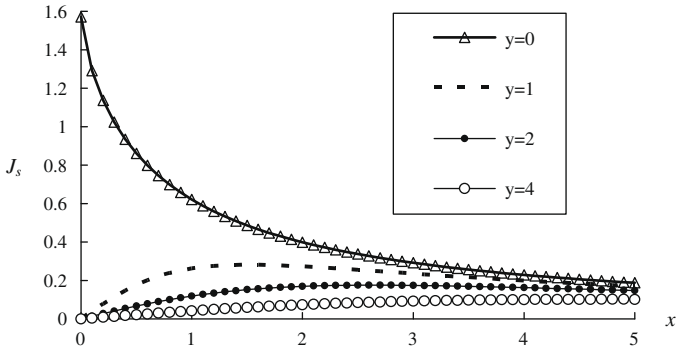

Fig. A2. Integral $J_s(x,y;a)$ for $a = 1$.

Eq. (B1) can be rewritten as

$$v(\mathbf{x}') = \int_A v^*(\mathbf{x},\mathbf{x}')f_2(\mathbf{x})dA + \int_L [v^*(\mathbf{x},\mathbf{x}')q(\mathbf{x}) - v(\mathbf{x})q^*(\mathbf{x},\mathbf{x}')]dL \tag{B2}$$

where $\partial/\partial n = n_i\partial/\partial x_i$ on an arbitrary boundary has been noticed, with n_i being the directional cosine of the outward normal, and we have denoted $q = \sigma_{2i}n_i = \mu(\partial v/\partial x_i)n_i$.

Eq. (B2) is valid when the source point $\mathbf{x}'$ is in the interior of the domain. Following the standard procedure of BEM, we need to move the source point to the boundary. Denote the plane boundary $x_3 = 0$ as L_0 and the remainder, which may be associated with internal cracks, holes or inclusions, as L_1. The total boundary of the problem is $L = L_0 \cup L_1$ with $L_0 \cap L_1 = \emptyset$. On L_1, $v^*(\mathbf{x},\mathbf{x}')$ and $q^*(\mathbf{x},\mathbf{x}')$ exhibit the same singularities as those for the conventional elasticity problems as already pointed out in the text. On L_0, while $v^*(\mathbf{x},\mathbf{x}')$ still exhibits a weak logarithmic singularity, the stress component $\sigma_{21} = \sigma_{12}$ is no longer singular, and the stress component σ_{23} also exhibits a weak logarithmic singularity. Thus, we obtain

$$Cv(\mathbf{x}') = \int_A v^*(\mathbf{x},\mathbf{x}')f_2(\mathbf{x})dA + \int_L v^*(\mathbf{x},\mathbf{x}')q(\mathbf{x})dL - \int_{L_0} v(\mathbf{x})q^*(\mathbf{x},\mathbf{x}')dL - P\int_{L_1} v(\mathbf{x})q^*(\mathbf{x},\mathbf{x}')dL \tag{B3}$$

where C is the free term coefficient, which equals 1/2 on a smooth boundary except L_0 and is unit on L_0, and the symbol P denotes the Cauchy principle value (Brebbia and Walker, 1979; Gaul et al., 2003). Eq. (B3) is the so-called boundary integral equation, based on which approximate solutions can be obtained by the boundary element method. It is noted that, if the interior sources are absent (i.e. $f_2 = 0$), then the domain integral on the right-hand side of Eq. (B3) vanishes, and only the boundary of the domain is involved in the solution. When $f_2 \neq 0$, some special techniques can also be employed to transform the domain integral to the boundary integral (Gaul et al., 2003) to reduce the computational effort.

The boundary integral equation (B3) can be simplified further, by making use of the property of the half-space Green's functions derived in this paper. First, we rewrite Eq. (B3) as

$$Cv(\mathbf{x}') = I_A + \int_{L_1} v^*(\mathbf{x},\mathbf{x}')q(\mathbf{x})dL - P\int_{L_1} v(\mathbf{x})q^*(\mathbf{x},\mathbf{x}')dL + \int_{L_0} [v^*(\mathbf{x},\mathbf{x}')q(\mathbf{x}) - v(\mathbf{x})q^*(\mathbf{x},\mathbf{x}')]dL \tag{B4}$$

where $I_A = \int_A v^*(\mathbf{x},\mathbf{x}')f_2(\mathbf{x})dA$. On L_0, we have

$$q = \sigma_{23} = -p - \mu^s \frac{\partial^2 v}{\partial x_1^2}, \quad q^* = \sigma_{23}^* = -\mu^s \frac{\partial^2 v^*}{\partial x_1^2} \tag{B5}$$

where $p(x_1)$ is the external shear force applied on the material surface $x_3 = 0$, and the boundary equilibrium equations (12) through (14) have been utilized. Thus on L_0, besides the contribution from the external load, the two terms in the integral also do not vanish identically as in the conventional elasticity (Telles and Brebbia, 1981). But, by integration by parts, we find

$$\begin{aligned}
&\int_{L_0} [v^*(\mathbf{x},\mathbf{x}')q(\mathbf{x}) - v(\mathbf{x})q^*(\mathbf{x},\mathbf{x}')]dL \\
&= -\int_{L_0} v^*(\mathbf{x},\mathbf{x}')p(\mathbf{x})dL - \mu^s \int_{L_0} \left(v^* \frac{\partial^2 v}{\partial x_1^2} - v \frac{\partial^2 v^*}{\partial x_1^2} \right) dL \\
&= -\int_{L_0} v^*(\mathbf{x},\mathbf{x}')p(\mathbf{x})dL - \mu^s \left(v^* \frac{\partial v}{\partial x_1} - v \frac{\partial v^*}{\partial x_1} \right)_{-\infty}^{\infty} \\
&= -\int_{L_0} v^*(\mathbf{x},\mathbf{x}')p(\mathbf{x})dL
\end{aligned} \tag{B6}$$

The integration on the right-hand side of Eq. (B6) does not contain any unknown field variables and can be performed by using any appropriate numerical quadrature scheme. Thus, it is also no longer necessary to discretize the plane boundary in the BEM, and hence reduces the effort to a certain degree in the numerical calculation. By substituting Eq. (B6) into Eq. (B4), we obtain

$$C v(\mathbf{x}') = I_B + \int_{L_1} v^*(\mathbf{x},\mathbf{x}')q(\mathbf{x})dL - P\int_{L_1} v(\mathbf{x})q^*(\mathbf{x},\mathbf{x}')dL \tag{B7}$$

where $I_B = I_A - \int_{L_0} v^*(\mathbf{x},\mathbf{x}')p(\mathbf{x})dL$. It is seen that, if there is no any interior boundary, then the last two integrals in Eq. (B7) vanish, and the formulation becomes exactly the one by directly integrating the Green's function solution over the area (or boundary) on which the load is applied. The form of Eq. (B7) is almost identical to that in conventional elasticity (Telles and Brebbia, 1981), except the coefficient C, which equals 1 on L_0.

If there is no surface effect on the remaining boundary L_1, then the proceeding analysis is almost the same as that for the classical elasticity. Otherwise, the equilibrium/constitutive equations for a material boundary (Gurtin and Murdoch, 1975; Gaul et al., 2003) should be employed. Such equations, while not given here, provide linear relations between the stresses, displacements and their derivatives, as similar to those in Eq. (B5). These can be readily incorporated into the BEM formulations.

Once again, it is emphasized that since the singularities of the Green's functions encountered in the BEM for elastic bodies with surface effect are almost identical (except the stress surface Green's function) to those for elastic bodies without surface effect, the most available effective and efficient treatments in the BEM developed for classical elasticity can be directly employed to analyze problems involving surface effects.

References

Abramovitz, M., Stegun, I., 1964. Handbook of Mathematical Functions with Formulas, Graphs, and Mathematical Tables. Dover, New York.

Brebbia, C.A., Walker, S., 1979. The Boundary Element Technique in Engineering. Butterworths, London.

Cammarata, R.C., 1994. Surface and interface stress effects in thin films. Progress in Surface Science 46, 1–38.

Gaul, L., Kögl, M., Wagner, M., 2003. Boundary Element Methods for Engineers and Scientists. Springer, Berlin.

Gibbs, J.W., 1961. The Scientific Papers of J. Willard Gibbs, vol. I, Thermodynamics. Dover, New York.

Gurtin, M.E., Murdoch, A.I., 1975. A continuum theory of elastic material surfaces. Archive for Rational Mechanics and Analysis 57, 291–323.

Gurtin, M.E., Murdoch, A.I., 1978. Surface stress in solids. International Journal of Solids and Structures 14, 431–440.

He, L.H., Li, Z.R., 2006. Impact of surface stress on stress concentration. International Journal of Solids and Structures 43, 6208–6219.

He, L.H., Lim, C.W., 2006. Surface Green function for a soft elastic half-space: influence of surface stress. International Journal of Solids and Structures 43, 132–143.

He, L.H., Lim, C.W., Wu, B.S., 2004. A continuum model for size-dependent deformation of elastic films of nano-scale thickness. International Journal of Solids and Structures 41, 847–857.

Kim, C.I., Schiavone, P., Ru, C.Q., 2010. The effects of surface elasticity on an elastic solid with mode-III crack: complete solution. Journal of Applied Mechanics 77, 021011.

Koguchi, H., 2008. Surface Green function with surface stresses and surface elasticity using Stroh's formalism. Journal of Applied Mechanics 75, 061014.

Li, Z.R., Lim, C.W., He, L.H., 2006. Stress concentration around a nano-scale spherical cavity in elastic media: effect of surface stress. European Journal of Mechanics, A/Solids 25, 260–270.

Lim, C.W., He, L.H., 2004. Size-dependent nonlinear response of thin elastic films with nano-scale thickness. International Journal of Mechanical Science 46, 1715–1726.

Lim, C.W., Li, Z.R., He, L.H., 2006. Size dependent, non-uniform elastic field inside a nano-scale spherical inclusion due to interface stress. International Journal of Solids and Structures 43, 5055–5065.

Lü, C.F., Chen, W.Q., Lim, C.W., 2009a. Elastic mechanical behavior of nano-scaled FGM films incorporating surface energies. Composites Science and Technology 69, 1124–1130.

Lü, C.F., Lim, C.W., Chen, W.Q., 2009b. Size-dependent elastic behavior of FGM ultra-thin films based on generalized refined theory. International Journal of Solids and Structures 46, 1176–1185.

Miller, R.E., Shenoy, V.B., 2000. Size-dependent elastic properties of nanosized structural elements. Nanotechnology 11, 139–147.

Mindlin, R.D., 1963. High frequency vibrations of plated, crystal plates. In: Progress in Applied Mechanics. Macmillan, New York, pp. 73–84.

Ou, Z.Y., Wang, G.F., Wang, T.J., 2009. Elastic fields around a nanosized spheroidal cavity under arbitrary uniform remote loadings. European Journal of Mechanics, A/Solids 28, 110–120.

Telles, J.C.F., Brebbia, C.A., 1981. Boundary element solution for half-plane problems. International Journal of Solids and Structures 17, 1149–1158.

Wang, G.F., Feng, X.Q., 2007. Effects of surface stresses on contact problems at nanoscale. Journal of Applied Physics 101, 013510.

Zhao, X.J., Rajapakse, R.K.N.D., 2009. Analytical solutions for a surface-loaded isotropic elastic layer with surface energy effects. International Journal of Engineering Science 47, 1433–1444.